

Geophysical logging DAPGEO-02_500m, Delftse Hout



Geophysical logging DAPGEO-02_500m, Delftse Hout

Author(s)

Pieter Pauw

Edwin Obando Hernandez

Pieter Doornenbal

Geophysical logging DAPGEO-02_500m, Delftse Hout

Client	TU Delft
Contact	Mr prof. dr. Vardon
Reference	
Keywords	Geophysical logging, Geothermal Delft project

Document control

Version	0.1
Date	13-10-2022
Project nr.	11206144-002
Document ID	11206144-002-BGS-0003
Pages	34
Classification	
Status	final

Author(s)

	Pieter Pauw	
	Edwin Obando Hernandez	
	Pieter Doornenbal	

Summary

From February – May 2022 a 500 m deep borehole (DAPGEO-02_500m) was drilled at Tweemolentjeskade in Delft, The Netherlands, as part of the Geothermal Delft project (GTD) led by Delft University of Technology (TU-Delft). The main purpose of the borehole was to improve site characterization in relation to geothermal energy exploitation and storage, as well as radioactive waste disposal. This report describes the geophysical logging activities carried out by Deltares during the last three drilling phases (phases 2, 3, and 4) of the borehole, covering a depth range of about 230-495 m below ground level (bgl).

In phase 3 all planned logging tools could be deployed. 5 different tools were used, resulting in a total measuring time of almost one day (continuous logging). The following logging parameters were collected: Spectral Gamma Ray (SGR), Total Gamma Ray (GR), 8", 16", 32", 64" normal Resistivity (RES), Spontaneous Potential (SP), Single Point Resistance (SPR), 16" and 64" Induced Polarization (IP), Sonic P-wave velocity (SON), PS suspension (P and S wave velocities), Nuclear Magnetic Resonance (NMR), and Borehole deviation (DEV). In phases 2 and 4 considerably less tools were used, due to incompatible drilling diameter and tool unavailability. In phase 4 an acoustic borehole imager (ABI) and an electromagnetic (EM) -induction (IL) tool were used in the limestone (Ommelanden chalk).

Except for the upper ~100 m of the subsurface, marine Pleistocene, Neogene, Paleogene, and Cretaceous sediments are present along the depth of the borehole, covering different depositional environments. Up to 413.5 m bgl these sediments are mostly unconsolidated. Below, the Ommelanden chalk can be considered as rock. Naturally, P and S wave velocities are much higher here.

The logging data generally shows straightforward correlations, such as the NMR clay-bound porosity and the GR. Fining-up and coarsening-up sequences are readily recognized by these data. Together with the RES and IL measurements they can also be used to discern distinct clay layers which may be designated as aquitards.

The coring data can also be used to compare the derived parameters from the mechanical wave data (Sonic and PS suspension logging data; P and S-wave velocities) and the NMR data (porosity and permeability). Regarding the P and S-wave velocities, special attention should be given to the lower part of the Paleogene section (400-413.5 m bgl) and the upper part of the Cretaceous section / Ommelanden chalk, as processing of the velocities was difficult here. Regarding the NMR porosity and permeability, coring data comparison is important to check if the cut-off times (porosity) and the empirical relationships for the permeability derivation can be applied for the Neogene and Paleogene sediments and Ommelanden chalk.

The logging data generally resembles the cutting description but, evidently, much more variation can be observed in the logging data. The logging data further complement the cutting description by its ability to derive geophysical parameters (P and S wave velocities, porosity, and permeability). These data can be used to further study the seismic effects of deep geothermal energy exploitation and the potential for (seasonal) high temperature aquifer thermal energy storage (HT ATES) and radioactive waste disposal.

Contents

	Summary	4
1	Introduction	7
2	Geophysical well logging measurements; background information	9
2.1	Spectral and total gamma ray (SGR and GR)	9
2.2	Electrical Resistivity (RES), Single Point Resistance (SPR), Spontaneous Potential (SP), and Induced Polarization (IP)	9
2.3	Electromagnetic (EM)-induction (IL)	11
2.4	Sonic (SON)	11
2.5	PS suspension logging	11
2.6	Borehole deviation (DEV)	11
2.7	Acoustic borehole imager (ABI)	11
2.8	Nuclear Magnetic Resonance (NMR)	12
3	Methodology	13
3.1	Logging speed and tool deployment	13
3.1.1	Phase 2	13
3.1.2	Phase 3	13
3.1.3	Phase 4	15
3.2	Data processing	15
3.2.1	PS suspension and Sonic logging	15
3.2.2	NMR	17
3.3	Depth correction	17
3.4	Visualization of the lithology	18
4	Results	19
4.1	General geological setting	19
4.2	Lithological variations	19
4.2.1	Phase 2 (Appendix II)	19
4.2.2	Phase 3 (Appendix III)	20
4.2.3	Phase 4 (Appendix IV)	21
4.3	P and S wave velocities phase 3	21
4.3.1	P-wave velocity (Appendix I and III)	21
4.3.2	S-wave velocity (Appendix I and III)	22
4.4	Borehole deviation	22
5	Discussion	24
6	Acknowledgements	25

7	Bibliography	26
8	Appendix overview	27
	Appendix I: P-wave analysis of Sonic and PS suspension logging data	27
	Appendix II: Logging results Phase 2	27
	Appendix III: Logging results Phase 3	27
	Appendix IV: Logging results Phase 4	27
	Appendix V: Description of the logging data	27
A	Appendix I: P-wave analysis of Sonic and PS suspension logging data	28
B	Appendix II : Logging results Phase 2	29
C	Appendix III : Logging results Phase 3	30
D	Appendix IV: Logging results Phase 4	31
E	Appendix V: Description of the logging data	32

1 Introduction

This report describes the geophysical logging of the DAPGEO-02_500m borehole, located at Tweemolentjeskade in Delft, The Netherlands (Figure 1.1). The DAPGEO-02_500m borehole is part of the Geothermal Delft project (GTD¹) and has been drilled to 1) install a seismic monitoring station to study the seismic effects of deep geothermal energy exploitation and 2) better characterize the lithology and (hydro)geology, including the derivation of some geophysical properties of the upper 500 m of the subsurface to explore the potential for (seasonal) high temperature aquifer thermal energy storage (HT ATEs) and radioactive waste disposal. Delft University of Technology (TU-Delft) is the leading scientific organisation of the GTD project.

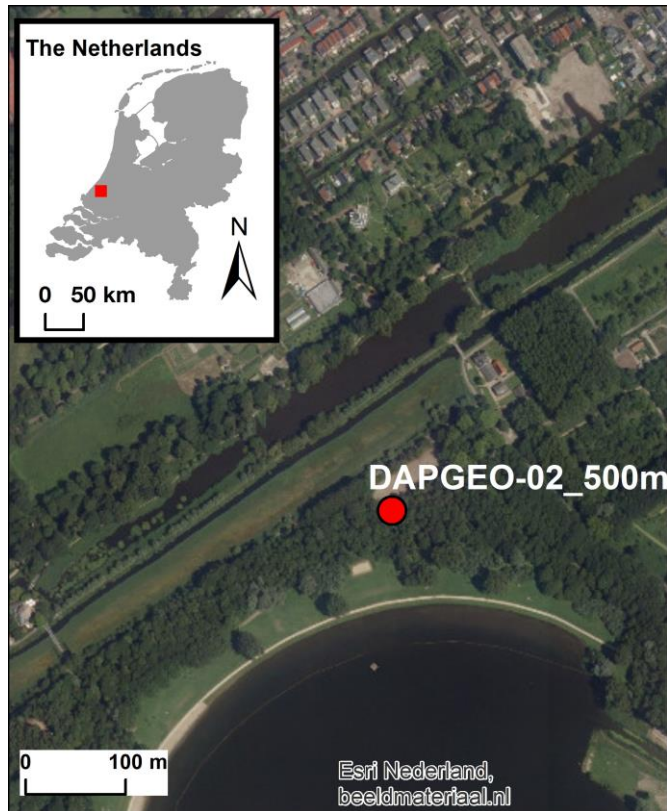


Figure 1.1: Location overview of the DAPGEO-02_500m borehole.

The drilling of the borehole took place during four different phases in the period February-May 2022. A rotary flush drilling method was used, and core samples were taken at pre-determined depths. Table 1 gives an overview of the phases, including the corresponding depth ranges, drill bit diameters, the most relevant² geophysical logging measurements, and the details of the logging tools applied. After each logging phase, a steel casing was placed in the open hole and inside the previous casing, and sensors were installed in the annular space of the open hole section. After sensor installation the annular space was backfilled with grout.

¹ Formerly known as Delft Aardwarmte Project.

² Only the logged parameters relevant for lithological and geological interpretation are used; logged data like input voltage, temperature, and elapsed time are considered irrelevant here.

Table 1.1: Overview of the different drilling phases, the most important geophysical measurements, and the corresponding tool types and tool manufacturers. The Century, Antares, and the QL40ABI tools are in-house (Deltares property), whereas the other tools have been rented.

Drilling phase	Depth range (m below ground level (bgl))	Drill bit diameter (mm)	Geophysical measurements	Corresponding tool type	Corresponding tool manufacturer
1	0-43	450	No logging carried out		
2	43-230.35	320	Spectral Gamma Ray (SGR) Total Gamma Ray (GR) 8", 16", 32", 64" Resistivity (RES) Spontaneous Potential (SP) Single Point Resistance (SPR) 16" and 64" Induced Polarization (IP)	QL40SGR QL40SGR QL40IP QL40IP QL40IP QL40IP	ALT ALT ALT ALT ALT
3	230.35-426.77	244	Spectral Gamma Ray (SGR) Total Gamma Ray (GR) 8", 16", 32", 64" Resistivity (RES) Spontaneous Potential (SP) Single Point Resistance (SPR) 16" and 64" Induced Polarization (IP) Sonic P-wave velocity (SON) PS suspension Nuclear Magnetic Resonance (NMR) Borehole deviation (DEV)	QL40SGR QL40SGR QL40IP QL40IP QL40IP QL40IP QL40FWS GeoVistaDPS BMR90 9622A	ALT ALT ALT ALT ALT ALT ALT GeoVista NM RSA Century
4	426.77-499	146	PS suspension Spectral Gamma Ray (SGR) Total Gamma Ray (GR) Electromagnetic (EM)-induction (IL) Acoustic Borehole Imaging (ABI)	GeoVistaDPS SGR1415 SGR1415 9512 QL40ABI	GeoVista Antares Antares Century ALT/Antares

Only phase 3 has been carried out as per our quotations³. In phase 1 no logging was planned nor carried out. The logging in phase 2 was limited to SGR, GR, RES, SP, SPR, and IP logging and took place within the [WarmingUP](#) project. In phase 4, PS suspension, SGR, GR, IL, and ABI logging data were collected instead of the anticipated suite of phase 3. The main reason for this was the drilling delay due to the detection of natural gas. Consequently, the BMR and QL40FWS tools were not available anymore. The selection of the alternative (mainly in-house) tools took place in consultation with TU-Delft.

This report has been kept rather concise, especially regarding the discussion of the results. Further analyses will be made once the results from the core sample analyses are finalized. The results described in this report can be used to focus the core sample analyses.

The results are presented graphically in Appendices I-IV. In addition, all raw data and field notes will be shared digitally in EXCEL, LAS and SEG2 format with TUD. Appendix V gives an overview of the raw and processed data.

³ 11206144-002-BGS-0002_v0.1 (February 25, 2022; PS and Sonic logging), 11206144-001-BGS-0003_v0.1 (June 11, 2021; Geophysical logging phases 3 and 4), and 11206144-001-BGS-0004_v0.1 (Processing and reporting phases 3 and 4).

2 Geophysical well logging measurements; background information

Most of the geophysical measurements have, except for some corrections like noise filtering and depth correction, not been further processed. For example, the Single Point Resistance (SGR) and Total Gamma Radiation (GR) have not been corrected for factors like borehole diameter of drilling fluid salinity. Nevertheless, these uncorrected measurements can be very useful to study lithological and (hydro)geological patterns.

For some measurements, the raw data were processed to derive some geophysical properties, such as the NMR hydraulic conductivity (by analysis of the T_2 distribution) or the Sonic P-wave velocity (by picking of the first P-wave arrival). Chapter 3 further explains how this processing was carried out and which other corrections have been taken place.

The remainder of this chapter briefly describes the most important geophysical measurements taken. More detailed information on these measurements can be found in well-known geophysical well logging reference works such as Ellis and Singer (2007), as well as on the websites of the various tool manufacturers Advanced Logic Technology (ALT), Antares, Century, GeoVista, and NM RSA (see Table 1.1). Here, also general information about the factors influencing the measurements, such as the drilling fluid invasion zone, borehole diameter, and tool centralization can be found.

2.1 Spectral and total gamma ray (SGR and GR)

The radioactive decay of ^{40}K , ^{232}Th , and ^{238}U in the subsurface leads to the emission of gamma radiation. Especially ^{40}K and ^{232}Th are generally associated with clay content, either by being part of the crystal structure or bound by the clay minerals. Hence, the higher the gamma radiation, the higher the clay content. There are, however, important exceptions; besides clay minerals, other minerals such as feldspars, glauconite, and K-rich evaporates like sylvite influence the gamma radiation. ^{238}U is generally more associated with organic deposits.

Most modern SGR and GR logging tools contain a scintillator, in which the incoming radiation induces light signals. These signals are processed by a photomultiplier tube into electrical pulses, which are then converted into a 'counts per second' (cps) unit. Factors like the scintillator size and type influence the registered cps. Therefore, a standard unit (API) has been developed, based on a calibration factory at the University of Houston (Belknap et al., 1978). All GR and SGR tools express the GR in API units nowadays.

SGR tools measure, in addition to the total gamma radiation, the total energy spectrum of the incoming radiation. Each isotope is associated with a specific energy level of the gamma radiation. For ^{40}K , this is 1.46 MeV, whereas the decay of ^{232}Th and ^{238}U takes place in series in which each decay event leads to a gamma radiation with a specific energy. From the total energy spectrum the contribution of the three isotopes can be deduced. This allows for a better analysis of clay content as well as mineral analyses.

2.2 Electrical Resistivity (RES), Single Point Resistance (SPR), Spontaneous Potential (SP), and Induced Polarization (IP)

The Electrical Resistivity (RES), Single Point Resistance (SPR), Spontaneous Potential (SP), and Induced Polarization (IP) are all electrical measurements. They are influenced by the

electrical properties of the porous medium as well as those of the pore fluid. The SP is the only measurement for which a current is not injected by the tool. Instead, only an electric potential is measured between two electrodes. SP is generally expressed in mV. The SP is essentially related to the diffusion of ions in the borehole fluid and the formation, and often mainly influenced by electrochemical forces. It develops when the salinity of the borehole fluid is different than the porewater fluid. Clayey zones act like an ion selective membrane and result in an SP anomaly.

The SPR is the total electrical resistance (in Ω) between the lower tool (current injection; A, see Figure 2.1) electrode and the upper part of the tool where the current electrode sink B is located. It is measured, just like the normal resistivity (see below), using a block wave current with changing polarity to prevent electrode polarization. The SPR is mostly influenced by the electrical resistance close to the current injection (A) electrode and is usually treated qualitatively to detect small changes in resistivity close to the current injection electrode, for example due to clay layers.

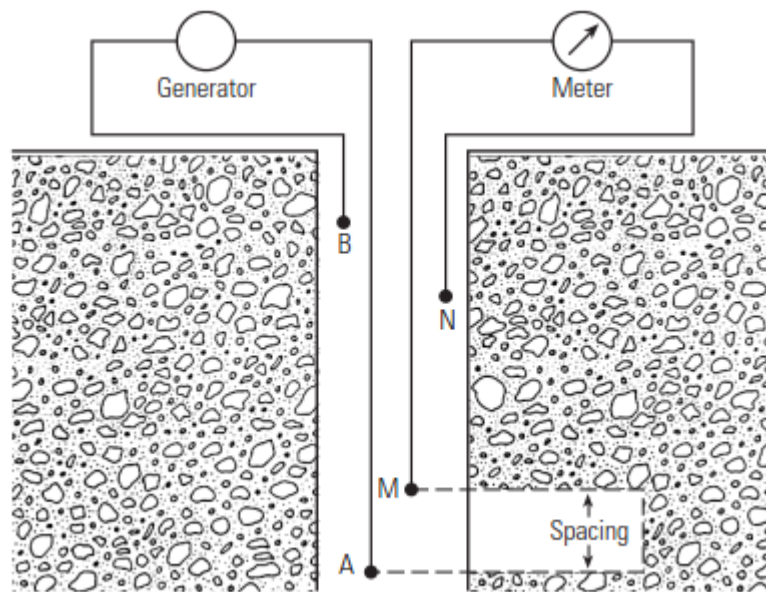


Figure 2.1: Concept of the electrode (ABMN) configuration of a normal resistivity tool. The distance AM is small compared to the other electrode distances. Many potential electrodes M can be present on the tool. The most known ones are the short and long normal, usually located at 16 and 64 inches from A.

'Normal' resistivity (RES) measurements rely on a relatively large distance between the four electrodes A, B (current) and M, N (potential), except for the distance AM, which is relatively small (Figure 2.1). The reference point for the electrical resistivity is halfway between the A and M electrodes. Historically, the 16 and 64 inch (AM distance) resistivity measurements have been denoted as 'short normal' and 'long normal' resistivity measurements. Also other AM distances can be used to deduce the influence of the borehole and invaded zone. With the QL40IP tool deployed in phase 3 (Table 1.1), N8 ('Normal'), N16, N32, and N64 normal resistivities were measured.

In addition to the RES measurements, IP measurements were carried out by measuring the voltage build-up (during current injection) and voltage drop-down (during current release) over time 16 (MA16) and 64 (MA64) inch potential electrodes respectively. This is used to determine the chargeability (Ma). In general, the higher the chargeability, the higher the clay content.

2.3 Electromagnetic (EM)-induction (IL)

Electromagnetic (EM) induction measurements rely on a high frequency alternating current generated in a transmitter coil, which leads to a primary EM field in the subsurface. Due to conduction, this field induces a secondary EM field, which is detected in a receiver coil. The alternating current measured in this receiver coil differs from the transmitted one in phase and amplitude, from which the electrical conductivity can be derived.

Sophisticated tools consist of several transmitter and receiver coils to increase the spatial resolution and improve the measurement of the electrical conductivity by compensating for the skin effect. The coil design is often such that the volume close to the tool does not have a significant contribution to the electrical conductivity, to prevent the borehole fluid have a large influence on the measurements. Evidently, the larger the borehole, the larger its influence. In this study, only compensated (skin effect-corrected) IL measurements were used. The Century 9512 EM-induction tool was deployed, only in phase 4.

2.4 Sonic (SON)

With a Sonic tool a sound wave is transmitted by a piezoelectric. The wave is detected at some distance from the transmitter. In its simplest configuration, two receivers are used. From the difference in arrival time at the two receivers the P-wave velocity can be determined, thereby aiming to exclude the effect of the borehole. Modern tools consist of more receivers. Moreover, they often record the full waveform from which, depending on the conditions, also shear (S) and Stoneley waves can be determined.

The QL40FWS deployed in phase 3 consisted of one transmitter and three receivers. Only the first two receivers were used for further analysis of the P-wave velocity.

2.5 PS suspension logging

The PS suspension logging tool from GeoVista provides measurements of P and S-waves. Compared to the Sonic logging tool, the P-source is different of nature (dipole source), has a lower frequency, and has more power. The P-wave receiver is a high frequency (~kHz) piezo electric device and the S-wave is a low frequency (~Hz) geophone receiver. This means that P and S – waves are recorded using different sampling frequency and duration. The dipole-source emits directional energy which is transmitted perpendicular to the wall of the borehole and generates shear waves within the formation.

2.6 Borehole deviation (DEV)

Borehole deviation measurements are carried out using magneto- and inclinometers to determine the inclination of the tool relative to the earth's gravitational vector and the orientation of the dip relative to the magnetic north. Hence, in a steel casing, only the inclination can be determined. The inclination and azimuth measurements are used to derive the path taken by the tool. This, for example, allows for a total vertical depth analysis, and a borehole trajectory derivation.

2.7 Acoustic borehole imager (ABI)

Acoustic borehole imagers (QL40ABI manufactured by ALT) make use of an ultrasonic signal. Near the top of the tool, an ultrasonic beam is sent in the coaxial direction of the tool, where at some point it is reflected 90 degrees by a mirror and send towards the borehole wall. The mirror is rotating, resulting in many datapoints per measurement depth. From the

recorded travel time and amplitude of the reflected signal a high-resolution (calliper) image of the borehole wall or casing can be derived.

The quality of the image depends to a large extent on the reflection coefficient, which depends on the densities and velocities of the borehole fluid and formation. The larger the contrast between the borehole fluid and the formation, the better the data quality.

2.8 Nuclear Magnetic Resonance (NMR)

NMR is a relatively new technique in geophysical logging for hydrogeological purposes. Hydrogen nuclei possess both magnetic moment and angular momentum. When subjected to an external magnetic field \mathbf{B}_0 , the combination of these properties leads to precession of the nuclei around the direction⁴ of the external magnetic field. One can imagine this situation as the nuclei acting like tiny gyroscope, with the rotating axis parallel to \mathbf{B}_0 . The frequency of the precession is known as the Larmor frequency, which is proportional to the gyromagnetic ratio (nucleus-specific) and the strength of the external magnetic field. The time it takes to reach 63% alignment of the precessing hydrogen nuclei (polarization) is referred to as T_1 .

Following the T_1 polarization, the hydrogen nuclei are tipped by another magnetic field \mathbf{B}_1 to a transverse plane relative to \mathbf{B}_0 . The tipping takes place in the form of a series known as the Carr-Purcell-Meiboom-Gill (CPMG) pulse sequence. Between the pulses, an 'echo' EM signal is measured by an antenna. Over the course of the pulses the EM signal decays over time, reflecting relaxation processes of the spinning hydrogen nuclei. This relaxation process is referred to as the T_2 relaxation. Because of their abundance and their intrinsic magnetic moment and angular momentum, hydrogen nuclei give by far the most dominant signal compared to other nuclei during the T_1 and T_2 processes.

In absence of metallic particles in the porous medium, both T_1 and T_2 are mainly influenced by surface relaxation processes taking place close to the mineral-water surface. The ratio of the surface relative to the volume of a pore controls the surface relaxation. From the T_2 distribution the total porosity, clay-bound water, capillary bound water (specific retention), and free water (specific yield) can be derived by inversion of the T_2 decay curve, assuming 'cutoff times' to specify the different contributions. The cutoff times may be dependent on the structure of the porous medium (and, hence, the lithology) and can be determined experimentally.

After defining the different contributions of the clay-bound, capillary bound, and free water, the hydraulic conductivity can be derived using empirical formulas. This is explained further in the next chapter.

⁴ Parallel or anti-parallel, depending on the energy state of the nucleus.

3 Methodology

The Century, Antares, and the QL40ABI tools that were applied are Deltares property (inhouse tools), whereas the other tools were rented. The necessary hardware adjustments on the winch, depth encoder, and tension were made in June 2021 (ALT / NMRSA tools) and a week before the logging of phase 3 (GeoVista PS suspension logging tool).

Although previously checked, the tension could not be recorded for the ALT/NMRSA tools. Tension could also not be recorded for the GeoVista tool due to a lack of time; the tool could just be shipped about a week before the start of the logging of phase 3. The tension could, however, be displayed real-time by using the Antares hardware parallel to the ALT, NMRSA, and Geovista tool runs. For the Century tools neither tension recording nor monitoring was available.

3.1 Logging speed and tool deployment

3.1.1 Phase 2

Logging during phase 2 took place on March 10 in the evening/night. A single logging tool combination was used; the QL40SGR tool was stacked on the QL40RES-IP tool from ALT. The tool was not centralized. The logging speed was up to 2 m/min in the open hole section lower than 190 m below ground level (bgl), where some clay layers were found. Total logging time was about 4 hours.

3.1.2 Phase 3

For phase 3 a total of 5 logging tools were used. The continuous logging activities together took about 24 hours. On March 26 in the evening (Figure 3.1), the deviation logging started using the Century 9622A tool. Logging speed did not exceed 9 m/min and the tool was not centralized.



Figure 3.1: Impression of the logging setup in phase 3.

Subsequently, in the night of March 26-27, the PS suspension logging tool from GeoVista was deployed, followed by the QL40FWS Sonic tool by ALT in the morning of March 27. The acquisition parameters utilized with both systems are described in Table 3.1.

Table 3.1: PS suspension and Sonic tool settings.

System/Parameter	Sonic logging	PS Logging	
Type of survey	P-wave	P - wave	S-wave
Record duration (ms)	4	20	80
Sampling frequency (kHz)	250	100	25
Depth interval (m)	0.05	0.5 -1.0	0.5-1.0
Depth range (m)	228 - 425	229 - 422	229 - 422
Data format	*.las	*.Seg2	*.Seg2

The PS logging tool of GeoVista followed the deviation run and was deployed using centralizers. Before starting the actual measurements, a few test measurements were performed to define the sampling frequency/record duration as well as the power of the source so the amplitudes of the signals were not clipped. Once the record duration, sampling frequency, and energy of the source were defined the measurements started. Each record consists of a single file of 6 traces. Traces 1-2 are the S-wave near receiver for left and right shots, traces 3-4 are the S-wave far receiver for right and left shots, and traces 5-6 are the P-wave near and far receivers. The S and P-wave time difference and the known distance between the receivers provides the point (interval) P-wave velocity (V_p) referenced to the middle point of the two receivers. With this system 2 depth intervals were utilized: 1.0 m from 234 m - 362 m, and 0.5 m from 362.0 m – 424.0 m. In the raw data, the depth reference is the tool top. In the processed SEG2 files, the reference is midway the two receivers (1.7 m from the tool top).

During the acquisition a field quality check was performed by visually inspecting the signals; the S-wave should depict clear and coherent cycles for both near and far receivers, as well as in phase of both positive and negative polarity signals. The P-wave traces should provide very clear first breaks (easy for picking) for both near and far receivers. During the survey a single measurement was recorded at each measuring position and were repeated only when both S and P wave did not depict the quality parameters previously described.

For the Sonic survey the actual acquisition is much faster because measurements are taken automatically while the tool is moving. Dedicated centralizers were used to keep the tool (QL40FWS) centered in the borehole. Data were recorded every 5.0 cm providing a resolution 10-20 times higher compared to PS suspension logging. Up to 3945 traces were recorded in total. Logging speed did not exceed 4 m/min.

Following the Sonic, a stack of the BMR90 (NM RSA) and QL40SGR (ALT) tools was deployed using centralizers. Logging speed was 1 m/min. Online support was provided by NM RSA.

The last run was performed using the QL40RES-IP tool, without centralizers and with a logging speed of about 5 m/min.

3.1.3 Phase 4

Logging of phase 4 commenced on May 11 in the morning with the EM-induction tool 9512A of Century, without centralizers and a logging speed up to 8 m/min. This was followed by the ABI using the QL40ABI modified by Antares, with centralizers equipped and a speed of 1 m/min. This tool was also used to measure the deviation of the borehole.

Following the ABI, the PS logging tool was deployed in a similar way as in phase 3, except for the centralizers. These were not used because of the relatively small diameter of the borehole. Finally, the SGR Antares tool was utilized with a measuring speed of 1-2 m/min and without centralizers.

3.2 Data processing

The data handling and processing was carried out with in-house Python scripts and open source tools such as Obspy ([ObsPy Documentation \(1.3.0\) — ObsPy 1.3.0 documentation](#)) and Lasio ([lasio - Log ASCII Standard \(LAS\) files in Python — lasio 0.30 documentation](#)). For the NMR, data was processed using the commercial software WellCAD. The NMR processing was carried out by NMRSA.

WellCAD was also used to process the P and S wave data. In the following subsections, some details of the PS suspension, Sonic, and NMR processing are described.

3.2.1 PS suspension and Sonic logging

P-wave processing for both Sonic and the PS suspension logging data was carried with a semblance approach, using the Velocity Workspace of the commercial logging software WellCAD. The semblance approach relies on cross-correlation and considers the amplitude of the waves. Using a Slowness-Time-Coherence (STC) plot (Figure 3.2), the maximum correlation can be chosen, which corresponds to a slowness. The P-wave velocity is calculated as the reciprocal of the slowness.

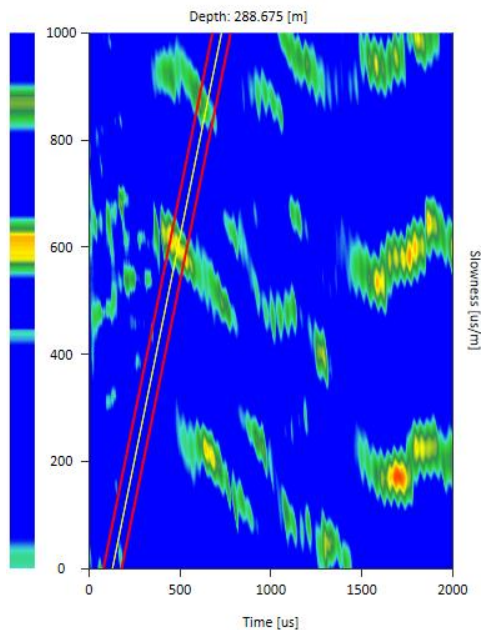


Figure 3.2: Example of a Slowness-Time-Coherence plot as used to pick the P-wave velocity. The colors indicate the correlation (scale 0-1). The yellow line is the so-called 'Mudline', which depends on the tool configuration (distance between the receivers and the diameter of the borehole). The red lines can be set to define a range in which the highest correlation is determined.

A similar approach was used for the S-waves. The velocities were checked with a velocity picking approach based on manually picking the first onset of opposite-polarity waves; the first S-wave cycle should be complementary meaning that both S-wave cycles of left-to-right and right-to-left records depict very similar shapes, but with opposite polarity. One example of an S-wave record with two signals of opposite polarity is presented in Figure 3.3 (top for near receiver and bottom for far receiver).

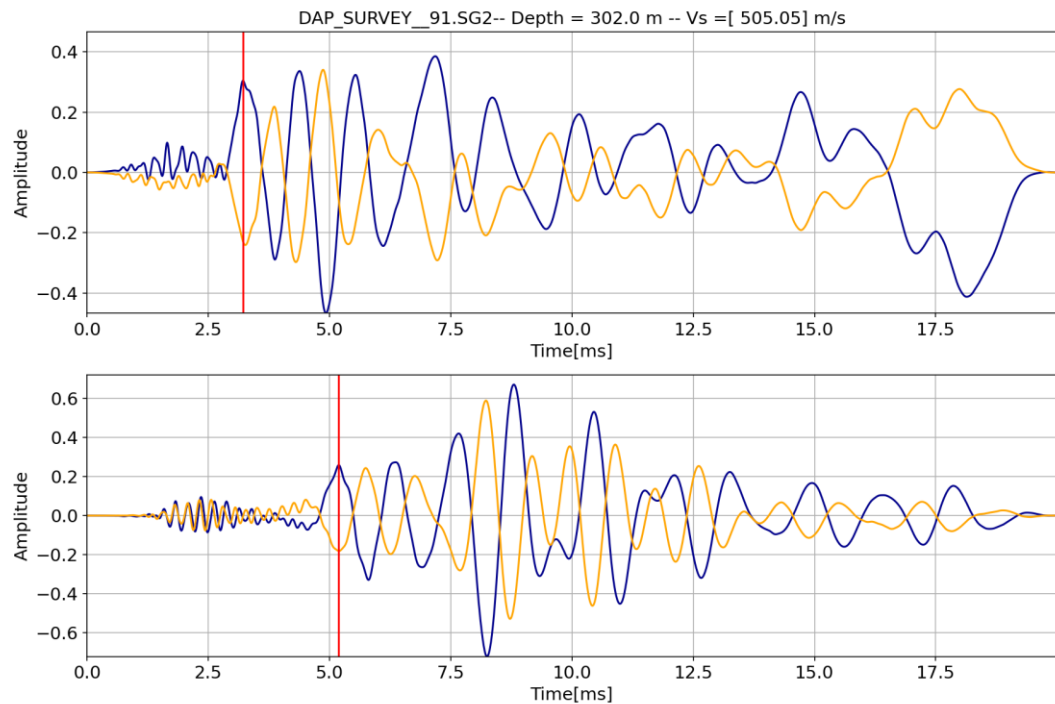


Figure 3.3: Example of manual S-wave picking using the first onset of opposite-polarity waves.

The manual picking led to reasonable results in the upper part of the section of phase 3. From about 360 m bgl, however, picking was much less evident which resulted in very low, unrealistic velocities (Vogelaar, 2022). Therefore, an alternative approach using an STC plot was chosen.

A summary of the processed Sonic and PS logging data is given in Appendix I. Here, the following data are displayed:

- Amplitudes of the incoming waves of the Sonic tool for the three receivers. Note that the measuring point is the transmitter (default value of the tool). This also holds for RX1-1A (closest receiver of the Sonic) in Appendix III. The distance from the transmitter to the three receivers is 60, 80, and 100 cm. The offset between the transmitter and the calculation of the Sonic P-wave velocity is therefore 70 cm.
- The frequency spectrum of the first receiver (at 60 cm from the transmitter). Again, here the reference point is the transmitter.
- The velocity analysis of the Sonic data (coherence analysis).
- The P-slowness and P-velocities of the Sonic and PS logging data, as well as the S-slowness and S-velocities. The reference point is halfway between the two receivers. For the S-waves, the analysis was split in two parts, which was related to a change in measurement interval at 360 m bgl. The data marked with ‘_1’ refers to the upper section where a 1-m interval was deployed, whereas ‘_2’ refers to the lower section with an interval of 0.5 m.
- The Poisson ratio of the Sonic (P-wave velocity) and PS suspension logging tool (S-wave velocity) data.

The analysis in Appendix I is restricted to phase 3, as in phase 4 only PS suspension logging data was collected, and only for a limited depth range. The results of the S- and P-wave velocities can be found in Appendix IV.

In Appendices I, III, and IV, the P-wave velocity from the Sonic tool is abbreviated with 'V P-wave Sonic'. Likewise, the PS suspension logging P-wave velocity is denoted with 'V P-wave PS'. For the shear waves in phase 3, two separate STC analyses were carried out due to the change in measurement interval around 360 m bgl. The upper and lower sections are denoted with 'V S-wave PS_1' and 'V S-wave PS_2', respectively.

3.2.2 NMR

Basic NMR processing was done using the following cutoff times:

- Clay Bound Water (CBW): 3 ms.
- Capillary water (CAPW): 33 ms until 413 m bgl and 100 ms below (carbonate section).
- Free water: 3 s

Standard coefficients for two permeability equations were applied for the respective lithology highlighted in the T_2 distribution track. These two equations are referred to as the Timur-Coates permeability (k_{TIM}):

$$k_{TIM} = a \cdot TPOR^m \cdot \left(\frac{FFV}{BFV} \right)^m \quad (1.1)$$

with coefficients $a=1$, $m=4$, and $n=2$, and the Schlumberger Doll Research permeability (k_{SDR}):

$$k_{SDR} = a \cdot TPOR^m \cdot T_{2LM}^n \quad (1.2)$$

with coefficients $a=4$, $m=4$, and $n=2$. BFV is the sum of CBW and $CAPW$. T_{2LM} is the geometric mean of the T_2 distribution. $TPOR$ is the porosity inferred from the NMR data. Both equations express the permeability in millidarcy (mD).

The corresponding hydraulic conductivity K is calculated using:

$$K = \frac{k \rho g}{\mu} \quad (1.3)$$

where g is the Earth gravitational constant, ρ is the fluid density, and μ is the fluid dynamic viscosity. Note that k needs to be converted from mD to m^2 .

3.3 Depth correction

The Century deviation and EM-induction runs appeared to not register the depth correctly. The raw depth data were therefore corrected using the gamma ray from the other tools as a reference. This resulted in an accurate depth correction.

In addition, in phase 2 a lowering of the pulley was observed at the end of the downward run. At the end of the upward run, a difference of 0.4 m was observed. This has also been corrected. The correction confirmed the end depth of the casing by a rapid decrease of the N8 resistivity.

Finally, the PS suspension logging data of phase 4 was corrected using the known depth of the casing foot. The reason for the incorrect depth registration was attributed to the high

drilling mud density, resulting in an almost floating tool. Around 440 m bgl the measurements were stopped to avoid risking tool loss.

3.4 Visualization of the lithology

The lithological description of the drilling company has been plotted together with the logging results. Five main lithological classes were used. The subdivision of the different classes is presented in Table 3.2. Likewise, the subdivision of the different admixtures is shown in Table 3.3. Not all admixtures were used⁵; only those that were regarded as important for log response.

Table 3.2: Main lithological classes as used for visualization and corresponding lithological classes as used by the drilling company.

Main lithological class for visualization	Included main lithological classes drilling company (in Dutch)
Clay	Klei
Medium fine sand	Fijn zand; matig fijn zand
Medium coarse sand	Matig grof zand
Coarse sand	Zeer grof zand
Limestone	Krijt

Table 3.3: Main admixtures as used for visualization and corresponding admixtures as used by the drilling company.

Main admixture for visualization	Included admixtures drilling company (in Dutch)
Very clayey	Sterk kleiig
Moderately clayey	Matig kleiig; met klei en kleisteen
Weakly clayey	Zwak kleiig; fijne grijze kleilaagjes
Very sandy	Sterk zandig
Moderately sandy	Matig zandig, matig grindig
Weakly sandy	Zwak zandig
Chert	Matig silex; Veel silex

⁵ Not used were admixtures such as silt, ('siltig'), moderately gravelly ('matig grindig'), organic matter ('humeus'), shells ('schelpen'), claystone (kleisteen), and low chert content (weinig silex).

4 Results

4.1 General geological setting

Different geological formations are encountered along the total depth range of the well logging. An indication of the depth range of these formations and their corresponding period or epoch is given in Table 4.1. Note that these boundaries are indicative; definite geological subdivision is better possible using the cores taken during the drilling. The remarks are the main output of the analysis of the logs and the interpretation based on the geological expertise.

Table 4.1: Overview of the different geological formations encountered in the logged depth range, including their corresponding period/epoch, drilling phase, depth range, as well as some remarks on the main lithological characteristics.

Geological formation(s)	Period/epoch	Depth range (m bgl)	Phase	Remarks
Waalre and Maassluis	Pleistocene	40-230	2	Top part perhaps part of the Urk formation. Important clay layers. Lower boundary with Oosterhout based on shell content.
Oosterhout and Breda	Neogene	230 – 359	3	A relatively high glauconite content in the sediment (elevated GR) compared to the Maassluis formation. Lower boundary towards the clay is based on clear increase in GR and NMR clay bound water.
Rupel (top section), bottom section unclear	Paleogene	359-413.5	3	From 359 – 394 bgl: relatively high GR, chargeability, and clay- and capillary-bound water. Below, a sandy section marking transition from upper to lower clay sequence is present; sharp decrease in GR, increase in resistivity and free water NMR. From 401-413.5 a fining up can be recognized (towards the base: decreasing clay content in NMR clay bound water, decreasing GR, decreasing chargeability, increasing resistivity).
Ommelanden	Cretaceous	413.5 – end depth	3/4	Clear decrease in GR compared to Paleogene section, increase in P and S wave velocities, no clay bound water. Relatively high chert content near the top, more clayey towards the bottom (increase of GR). Hard section between 480-484 m bgl.

The following section describes the lithological variations based on the logging measurements and cutting samples per phase.

4.2 Lithological variations

4.2.1 Phase 2 (Appendix II)

The casing foot, marking the end depth of drilling phase 1, can be easily recognized by a jump in electrical resistivities and a sharp decrease of the chargeability at about 42 m bgl. From this depth to about 103 m bgl sediments of the Waalre formation are present, except for perhaps the top few meters (Urk formation). In general, these sediments are of fluvial origin. Increasing clay content and clay layers in this section can be recognized by higher GR and (to a lesser extent) chargeability. Also, the SPR, SP, and electrical resistivities generally correlate with the clay content (e.g., around 90 m bgl), but they are also influenced by the

drilling fluid and porewater salinity. The normal resistivities (RES), for example, show a general decrease with depth, which is probably related to an increasing salinity of the groundwater. While the N64 does show this trend, it does not seem to react much on clay layers, even when they are relatively thick. The reason behind this is unclear. In the following, the discussion will be predominantly on the other (N8, N16, and N32) RES measurements. Similarly, the longest electrode spacing used to determine the chargeability (MA64) appeared to be much less responsive than the shorter spacing (MA16), so the latter will solely be used from this point on.

Below 103 m bgl to the end depth of the drilling of phase 2, marine Pleistocene sediments are encountered. These sediments belong to the Maassluis formation. The clay content in the top part is relatively high, but from about 116 m bgl to the clay layer at 187 m bgl, the clay content seems to vary much less, as indicated by the GR and MA16. Fine sand is the dominant lithology in this section. The local increases in SPR and RES are interpreted as zones with coarser sand and/or higher shell content.

The Maassluis formation is present until the end depth of phase 2. The bottom part of this Maassluis section is rich in clay. A clear clay layer is present at about 187 m bgl, where an increase in GR and MA16, and a decrease in SP and SPR can be recognized. Below, a sandier section is found between 192 and 195 m bgl. From 195 m bgl to about 205 m bgl the GR indicates a general coarsening up sequence, intersected by some sandier sections (e.g., from 207-210 m bgl). Similarly, a second coarsening up section can be seen from 215 to the end of the borehole. A coarsening upward sequence in marine environments can be associated with an increase in depositional energy and a shallowing of the depositional environment (closer to the shoreline).

4.2.2 Phase 3 (Appendix III)

Below the Maassluis formation, the Oosterhout (top) and Breda (bottom) formations are present, according to regional geological data (REGIS, see www.dinoloket.nl). From 230 m to 268 m bgl, the GR values are generally increasing. This can be attributed to a general increase in clay content, especially towards the lower part of this unit as indicated by the clay-bound NMR contribution. Within this unit, local increases in chargeability, GR, and clay-bound NMR and decreasing resistivities indicate more clayey layers, whereas opposite patterns of these measurements (e.g., around 247 m bgl) indicate coarser (shell-rich) layers.

From 268 towards 280 m bgl a fining up sequence can be recognized; the clay-bound NMR, chargeability, and GR are all decreasing downwards. This may reflect a deepening of the depositional environment (relative sea level rise). The resistivity is decreasing with depth, which is probably related to an increasing porewater salinity. Below, between 280 and 295 m bgl, a rather heterogeneous zone is present, where a relatively high variability of locally decreasing resistivities, locally increasing MA16, NMR clay-bound water, and (to a lesser extent) GR values indicate layers with higher clay content. The base of this sequence consists of a clay-rich layer.

Between 295 m and 360 m bgl, the GR and clay-bound NMR values first increase and then decrease again, expect for the bottom section. The transition zone from increasing to decreasing values occurs around 320 m bgl. Here, the resistivities decrease and the chargeability increases clearly, while both were rather constant in the upper section. Free-water NMR values also increase considerably around 320 m bgl. Furthermore, 320 m bgl is also the zone where some indication of lithified clay was described by the drilling company. A coarsening-up(top)–fining-up(bottom) sequence could explain these patterns, but it remains

unclear why MA16 increases in the lower section towards the bottom. The decreasing trend of the resistivity could be explained by increase in porewater salinity.

A clear change in many geophysical logging measurements can be observed between 359 and 360 m bgl. Here, NMR clay-bound water, GR, and MA16 increase considerably. This marks the transition from Neogene (Breda and Oosterhout formations) towards Paleogene sediments. The Paleogene sequence has its base around 413.5 m bgl and consists of two clay-rich sections (360-393.5 m bgl and 401-413.5 m bgl), intermitted by a sandy section where the GR, clay-bound NMR, and MA16 values are lower.

The chalk belonging to the Ommelanden formation starts at 413.5 m bgl and is characterized by a low GR and no contribution of clay-bound NMR. The SPR and N8 and N16 resistivities coincide with local decrease in NMR porosity. Here, the chalk is probably denser and contains more chert. It remains unclear, however, why the N32 resistivity decreases at these levels.

4.2.3 Phase 4 (Appendix IV)

The last drilling phase (up to 499 m bgl) solely comprises the Ommelanden chalk. From 426 to about 475 bgl the chalk has a low clay content; GR values remain low. Below, the clay content increases, as does the GR. Remarkably, the IL resistivity goes up. This is probably related to a decrease in porosity and increasing rock strength. Especially between 480 and 484 m bgl, where the IL resistivity reaches the highest values, the acoustic log also shows the highest amplitudes.

The acoustic log is generally of poor quality. The diagonal lines appearing mostly in the radial image indicate a rotating behaviour. After a discussion with the drilling company, this pattern can most likely be attributed to the drilling (the roller bit), which leads to a local erosion of the borehole wall in a 'spiral'-like fashion. Both tool and processing of the data were checked to avoid erroneous interpretation of this signal.

Regarding the PS suspension logging data, there is a remarkable constant S-wave velocity in the logged section. The constant waveforms suggest that the tool might not have lowered at all to the desired depth. On the other hand, the tension readings didn't give an indication of a sudden tension drop. Rather, the values almost linearly decreased in the open hole section, just like the SGR run. P-wave velocities beyond 1500 m/s could not be retrieved from the data. It remains unclear what the reason behind this is. The presence of (natural) gas could be a possible reason. In Appendix IV, the P-wave velocities are not presented.

Due to the high density, and therefore buoyancy force of the drilling fluid, the PS suspension and SGR logging tools could not be lowered until the desired depth. The tension indicated that at some point both tools were almost floating. Due to the tight drilling scheme (permissions) and earlier gas leakage problems, it was decided to avoid risking tool loss and abandon the PS suspension and SGR logging runs earlier than planned.

4.3 P and S wave velocities phase 3

4.3.1 P-wave velocity (Appendix I and III)

Generally, the P-wave velocity doesn't vary too much between 230 and about 325 m bgl. The Sonic P-wave velocity closely resembles the P-wave velocity from the PS suspension logging tool. Locally decreasing velocity seems to correspond with a lower GR and (especially) a higher free-water NMR porosity. Also, below 325 m bgl one can observe decreasing P-wave velocities with increasing free-water NMR porosity.

In the Paleogene clays the P-wave velocity clearly decreases and does not correlate much more with the free-water NMR porosity. A local increase in P-wave velocity is present around 370 m bgl, where resistivities increase and total NMR porosity decreases. The increase in Sonic P-wave velocity is more pronounced than the PS suspension logging tool. Around 387 m bgl, the P-wave velocity increases, which is probably related to a decreasing porosity. Also here the Sonic and PS suspension logging tool results differ a bit.

Around 400 m bgl, the two P-wave velocities start deviating significantly. The PS suspension logging tool shows higher velocities, whereas the Sonic velocity remains relatively constant. At this depth, the semblance analysis of the PS suspension logging was uncertain and much less evident than the section above, in contrast to the Sonic semblance analysis. Hence, the Sonic P-wave velocity is probably more realistic in this section up to a depth of 410 m bgl, where the two appear similar again. The peak in P-wave velocity around 406 m bgl also nicely correlates with a decreasing NMR porosity and increase in resistivity. A few meters below this peak, the P-wave velocity significantly increases to values well above 2000 m/s. To some extent this can be attributed to porosity decrease, but the material is presumably also significantly less compressible.

In the chalk the P-wave velocity doesn't increase much further. Locally higher P-wave velocities indicated by the Sonic measurements correlate well with increases in resistivity and decreases in NMR total porosity.

4.3.2 S-wave velocity (Appendix I and III)

The S-wave velocity analysis was done in two parts. Above 360 m bgl, where the measurement interval was 1 m, the semblance analysis resulted a variation in S-wave velocity between 350 and 570 m/s. The general trend is an increase in velocity with depth. The calculated Poisson ratio (based on the Sonic P-wave velocity data) varies between 0.43 and 0.47.

Below, in the Paleogene clays, the S-wave velocity decreases in a similar way as the P-wave velocity. The lowest analysed velocity is about 316 m/s. In the lower part of the Paleogene clays the S-wave velocity clearly starts to increase around 408 m bgl. Here also the Sonic P-wave velocity increases. In the chalk the S-wave velocity is more stable. The peak in S-wave velocity at 414 m bgl is probably unrealistically high (~1897 m/s) and should be neglected. Consequently, the Poisson ratio is negative at this depth.

The Poisson ratio is high (up to 0.48) in the upper part of the Paleogene section. In the lower section from 408 m bgl below, the Poisson ratio clearly decreases, indicating that the bottom part of this clay section clearly has different geomechanical properties. It also shows much more variation, but this can be attributed to the variation of the Sonic P-wave velocity and the difference in measurement interval between the Sonic and PS suspension logging tool.

4.4 Borehole deviation

The result of the borehole deviation measurements is shown in Figure 4.1. A deviation of more than 8 m can be observed, generally in north-northeast direction. The section in the casing has been neglected, as directional measurements are meaningless here due to the disturbance of the Earth's magnetic field measurements. Between phases 3 and 4 a section of about 3 m was not measured and has been neglected. Note that both depth indicator of phases 3 and 4 start at the end of the casing and that the starting depth has also been indicated by a star. Hence, the first blue star corresponds to the bottom of the casing of phase 2, and the first red star corresponds to the first measurement carried out in the open section (~428 m).

Borehole deviation

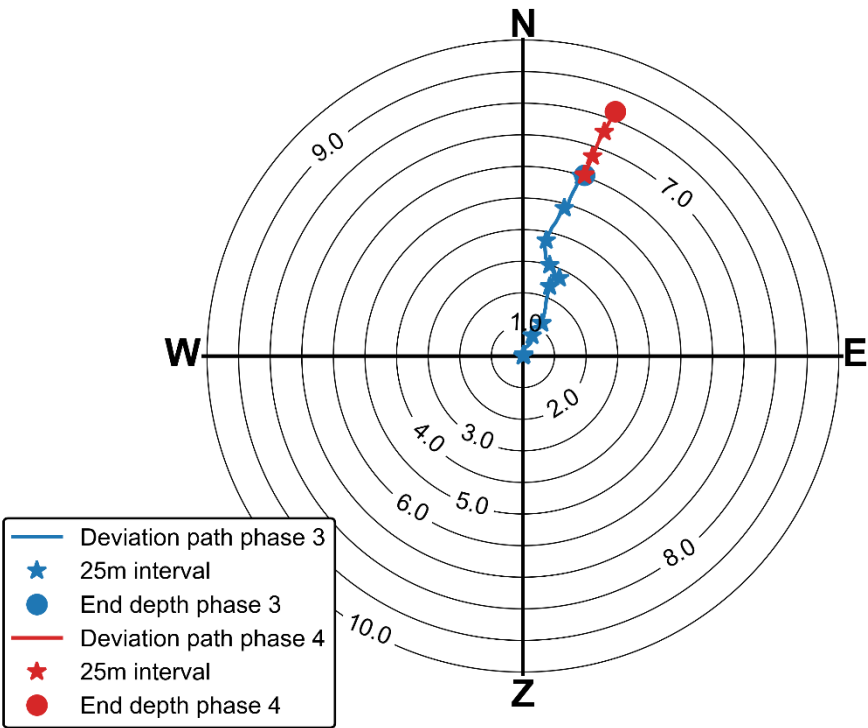


Figure 4. 1: Borehole deviation as measured in phases 3 and 4. Hence, the starting depth of this plot is around 230 m bgl.

5 Discussion

The logging data generally shows straightforward correlations, such as the NMR clay-bound porosity and the GR. Some patterns in other parameters remain unexplained. These can be further analysed using the coring data, for example to explain the opposing behaviour of the N32 normal resistivity around 414.5 m bgl and 416.5 m bgl compared to the other resistivities.

The coring data can also be used for comparison with the derived parameters from the mechanical wave data (Sonic and PS suspension logging data; P and S-wave velocities) and the NMR data (porosity and permeability). Regarding the P and S-wave velocities, special attention should be given to the lower part of the Paleogene section (400-413.5 m bgl) and the upper part of the Cretaceous section / Ommelanden chalk, as processing of the velocities was difficult here. Regarding the NMR porosity and permeability, coring data comparison is important to check if the cut-off times (porosity) and the empirical relationships for the permeability derivation can be applied for the Neogene and Paleogene sediments and Ommelanden chalk. To our knowledge, there has been very little NMR data collected in these formations so far in the Netherlands.

A possible other topic that could be studied using the coring data is to what extent the GR and SGR data are influenced by glauconite concentration. Glauconite complicates the interpretation of the GR data. Using the coring data, the influence of glauconite and different clay minerals on the total gamma radiation can be determined. Such an analyses can then be used to better characterized other (nearby) GR logging datasets.

The logging data generally resembles the cutting description but, evidently, much more variation can be observed in the logging data. The logging data further complement the cutting description by its ability to derive geophysical parameters (P and S wave velocities, porosity, and permeability). These data can be used to further study the seismic effects of deep geothermal energy exploitation and the potential for (seasonal) high temperature aquifer thermal energy storage (HT ATES) and radioactive waste disposal.

The collected datasets can be used for comparison with other geophysical datasets previously collected in the area of the Delftse Hout. At least the sandy section separating the two clay-rich Paleogene sections (360-393.5 m bgl and 401-413.5 m bgl) is also present in other geophysical data. Extensive comparison with other data is beyond the scope of this report and is left for further analysis by TUD.

6 Acknowledgements

The following persons are thanked to make the logging and processing of the data possible, especially with respect to their flexibility in relation to the tight drilling and logging schedule:

- Miel Kühr (Descona)
- Bruno Legros, Timo Korth (ALT)
- Ryan Gee (NMRSA)
- Mamdouh Barazi (GeoVista)

- Belknap, W.B., Dewan, J.T., Kirkpatrick, .C.V, Mott, W.E., Pearson, A.J., Rabson, W.R., 1978. API calibration facility for nuclear logs. Gamma ray, neutron density logging, SPWLA Repr. Pap. E.
- Ellis, D.V., Singer, J.M., 2007. Well Logging for Earth Scientists. Springer, Dordrecht, The Netherlands.
- Vogelaar, L., 2022. Geophysical well-logging at Delftse Hout for DAP well. TU Delft University of Technology.

8 Appendix overview

Appendix I: P-wave analysis of Sonic and PS suspension logging data

Appendix II: Logging results Phase 2

Appendix III: Logging results Phase 3

Appendix IV: Logging results Phase 4

Appendix V: Description of the logging data

A Appendix I: P-wave analysis of Sonic and PS suspension logging data

B Appendix II : Logging results Phase 2

C Appendix III : Logging results Phase 3

D Appendix IV: Logging results Phase 4

E Appendix V: Description of the logging data

In Table V an overview of different LAS files containing the logging data is given, including Log Definitions (LAS3) or column names/Curve Information (LAS2) which correspond to the data (headers) in Appendices II-IV. Table V also contains a reference to the PS suspension logging data of phases 3 and 4 (SEG2 files).

Table V: Overview of the different LAS2, LAS3 and SEG2 files containing the logging data. The Log Definition (LAS3) and column name (LAS2) can be used to look up the corresponding measurement in the LAS files from the header in Appendices II-IV.

Name of datafile	Drilling phase	Log Definition (LAS3) or column name (LAS2)	Description and unit
DAPGEO-02_500m_PHASE2_RES_IP_SGR.las	2	GR K TH U N8 N16 N32 N64 SP SPR MA16 MA64	Total gamma ray (API) Potassium content (%) Thorium content (ppm) Uranium content (ppm) 8" normal resistivity (Ω m) 16" normal resistivity (Ω m) 32" normal resistivity (Ω m) 64" normal resistivity (Ω m) Spontaneous Potential (mV) Single Point Resistance (Ω) 16" chargeability (ms) 64" chargeability (ms)
DAPGEO-02_500m_PHASE3_RES_IP.las	3	N8 N16 N32 N64 SP SPR MA16 MA64	8" normal resistivity (Ω m) 16" normal resistivity (Ω m) 32" normal resistivity (Ω m) 64" normal resistivity (Ω m) Spontaneous Potential (mV) Single Point Resistance (Ω) 16" chargeability (ms) 64" chargeability (ms)
DAPGEO-02_500m_PHASE3_DEV_c.las	3	SANG SANGB	Inclination (degrees) Magnetic north deviation (degrees)
DAPGEO-02_500m_PHASE3_NMR_SGR_c.las	3	GR K TH U TPOR T2LM MOVEABLE_WATER CLAY_BOUND_WATER BOUND_WATER K_KSDR K_KTIM	Total gamma ray (gAPI) Potassium content (%) Thorium content (ppm) Uranium content (ppm) NMR Porosity (-) Geometric mean of the T_2 distribution (ms) Contribution moveable water to porosity (-) Contribution clay bound water to porosity (-) Contribution capillary bound water to porosity (-) Hydraulic conductivity (m/d) (Schlumberger Doll Research) Hydraulic conductivity (m/d) (Timur-Coates)
DAPGEO-02_500m_PHASE3_FWS.las	3	RX1-1A RX1-2A RX2-1A	Sonic wave amplitudes at the first receiver (-) Sonic wave amplitudes at the first receiver (-); long time window Sonic wave amplitudes at the second receiver (-)

		RX3-2A	Sonic wave amplitudes at the third receiver (-)
DAPGEO-02_500m_PHASE3_V PVS_processed.las	3	V_P-WAVE_SONIC V_P-WAVE_PS V_S-WAVE_PS_1 V_S-WAVE_PS_2	Processed P-wave velocity Sonic (m/s) Processed P-wave velocity PS suspension logging (m/s) Processed S-wave velocity PS suspension logging, upper section 1m interval (m/s) Processed S-wave velocity PS suspension logging, lower section 0.5 m interval (m/s)
p_near_phase3.sg2 p_far_phase3.sg2 s_near_l_phase3.sg2 s_near_r_phase3.sg2 s_far_l_phase3.sg2 s_far_r_phase3.sg2	3	-	P-wave data PS suspension logging tool, near receiver P-wave data PS suspension logging tool, near receiver S-wave data PS suspension logging tool, near receiver, left shot S-wave data PS suspension logging tool, near receiver, right shot S-wave data PS suspension logging tool, far receiver, left shot S-wave data PS suspension logging tool, far receiver, right shot
DAPGEO-02_500m_PHASE4_A BI.las	4	DEVIATION_ABI DRIFTAZIMUTH_ABI AMPLITUDES_NULL_2D RADIUS_NULL_2D	Inclination (degrees) Magnetic north deviation (degrees) ABI amplitude (db) ABI radius (mm)
DAPGEO-02_500m_PHASE4_S GR.las	4	K_SGR TH_SGR U_SGR	Potassium content (%) Thorium content (%) Uranium content (%)
DAPGEO-02_500m_PHASE4_I L.las	4	GAMMA (GR in Appendix IV) COND RES	Total gamma ray (API) Electrical conductivity, skin effect compensation (mS/m) Electrical resistivity, reciprocal of COND (Ω m)
p_near_phase4.sg2 p_far_phase4.sg2 s_near_l_phase4.sg2 s_near_r_phase4.sg2 s_far_l_phase4.sg2 s_far_r_phase4.sg2	4		P-wave data PS suspension logging tool, near receiver P-wave data PS suspension logging tool, near receiver S-wave data PS suspension logging tool, near receiver, left shot S-wave data PS suspension logging tool, near receiver, right shot S-wave data PS suspension logging tool, far receiver, left shot S-wave data PS suspension logging tool, far receiver, right shot
DAPGEO-02_500m_PHASE4_V S_processed.las	4	V_S-WAVE_PS	Processed S-wave velocity PS suspension logging

Deltares is an independent institute for applied research in the field of water and subsurface. Throughout the world, we work on smart solutions for people, environment and society.

Deltares

www.deltares.nl